Communications in Information and Systems
Volume 22, Number 4, 477–497, 2022

Contact detection algorithm for needle puncturing robot

T. Matsuno, N. Kido, T. Kamegawa, T. Hiraki, and T. Fukuda

There is a surgical method called Interventional Radiology (IR) in which needles and catheters are inserted into the body using image diagnostic techniques such as CT fluoroscopy and X-ray fluoroscopy images to perform percutaneous treatment. IR has been applied to various treatments including lung cancer treatment, liver cancer treatment, and biopsy. Since it is less invasive than conventional surgery, it is possible to leave the hospital within 3 to 4 days after surgery. Therefore, IR surgery has been receiving increasing attention in recent years. Doctors are, however, exposed to strong radiation in the case of under CT guidance. In order to overcome this problem, we developed remote-controlled IR assistance robot named as Zerobot. And in order to make the operation succeed regardless of the difference of techniques of doctors, we have studied an automated puncture system with the robot. During the automated motion, the collision of the robot with CT gantry should be avoided. In this report, a method to detect contact between Zerobot and CT gantry is proposed.

1. Introduction

There is a surgical method called Interventional Radiology (IR) that doctors insert needles or catheters into patients by using CT images or X-ray images. Prof. Fukuda et al. had developed the IR robot using catheter in early times for intravascular neurosurgery [1–4]. As one of his studies, a new prototype model of micro catheter with active guide wire that has two bending degrees of freedom is developed. Also, IR endovascular simulator for both of the medical training and the medical robot evaluation has been developed [5, 6]. The simulator can reproduce the forms of blood vessels of specified patients based on CT information of them, and has similarity of physical properties with human. The simulators are commercially sold under the name 'Eve' currently.

IR is applied to biopsy and the treatments for lung cancer and liver cancer [7]. Currently, doctors perform IR operation with manually holding

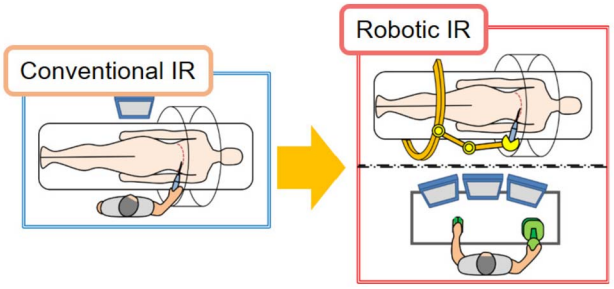

Figure 1: Concept of Robotic IR.

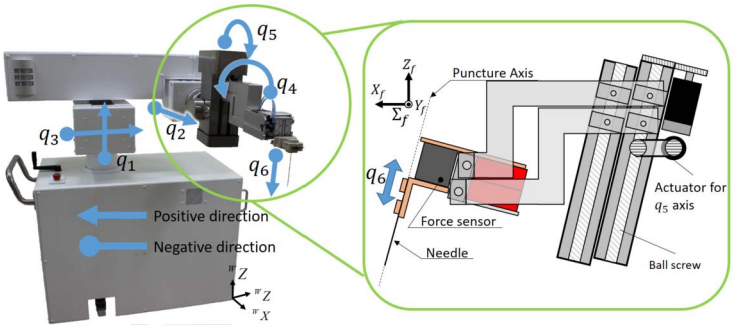

Figure 2: Appearance of Zerobot.

a needle to puncture under CT guidance. Also, doctors must control the position of needle carefully and accurately because tumors are about 5mm in diameter. In addition, doctors are exposed to radiation because they should perform IR close to CT equipment. In order to prevent radiation exposure, doctors wear radiation protection aprons and handle a needle using a forceps, which is useful to make distance between a hand of the doctor and CT measure plane. It is, however, impossible to prevent radiation exposure perfectly. Hence, some medical robots are developed in order to reduce radiation exposure, such as AcuBot [8], CT-Bot [9] and MAXIO [10]. We also proposed a robotic IR concept that doctors operate a puncture robot by remote control and perform IR so as to reduce doctors' exposure as shown in Fig. 1. The robot named as Zerobot is developed for needle insertion with teleoperations by a doctor is in version 3.1, which is shown in Fig. 2. In this study, in order to seek the problem of Robotic IR system, we have conducted phantom puncture experiment and animal puncture experiment [11].

Currently, a needle is inserted using Zerobot, while the doctor observes

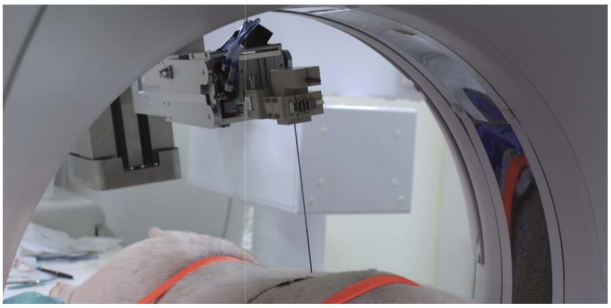

Figure 3: Working space for insertion needle.

real-time CT imagery. However, the following elements will be changed by doctor's skill to operate the robot.

1) Surgical time will be longer.
2) Patient's radiation exposure will increase.
3) Hitting rate to the tumors will decrease.

In order to have a surgery with the robot safely, it is required that an automated system insert a needle without the skill of doctors. One problem when introducing the automated puncture is narrowness of working space. Figure 3 shows the appearance of animal experiment with a long biopsy needle. When using a longer biopsy needle, there is possibility for Zerobot to contact a part of CT gantry. If contact of them occurs, the surgery should be stopped immediately. In order to avoid the collision between Zerobot and CT gantry during the automated puncturing, the algorithm to detect the contact between Zerobot and CT gantry is proposed.

Conventional studies of contact detection algorithm have progressed especially in the fields of computer graphics [12, 13], and they are applied to many applications. The framework for moving objects is called as continuous collision detection (CCD) [13], that is needed in virtual reality or game programing. In contrast, the contact detection for static objects is called as discrete collision detection, that is applied in this study. The base methods of them can be divided three types according to the element for shape approximation. (i) The sphere element type adopts method to calculate the distance between centers of two spheres so as to judge the contact condition [14]. Obviously the accuracy of contact judgment cannot be expected. (ii) The box element type adopts the method to make a minimum box which covers all edges of one object. Axis-aligned bounding boxes (AABB) approach is most easy method in box element type. It has shorter time in both of the shape

approximation and the contact judgment. Meanwhile, the accuracy of contact judgment is relatively rough with generating false positive under the condition with narrow gap. In order to improve the accuracy, the Oriented bounding box (OBB) is utilized. It has more complex contact judgment than AABB. (iii) The triangle element type has high accuracy but time consuming. Tomas proposed a method to utilize triangles of the object surface to calculate contact condition [15]. In advance, the surface of an object is converted into many triangles covering the object in this method. Some CAD software have this function, and we can set the precision of surface curvature in this process. Then, the contact judgment for all combination of triangles should be calculated. Therefore, the accuracy of contact judgment is controllable and becomes enough high, but calculation time extends due to increasing the number of triangles for the guarantee of precision.

Currently, so as to reduce the calculation time, two approaches are studied. One is utilizing GPU to realize parallel processing [13, 16]. The other is to introduce the hybrid method to reduce the number of paired triangles for contact judgment by utilizing bounding volume method [16, 17]. The sphere element type and the box element type belong to bounding volume method [12]. In the hybrid method, the tree or the hierarchy is used for expressing an object as combination of convex volume. The parts which obviously have no contact can be excluded from the calculation target in the early stage. Meanwhile, the combination of parts, which still have possibility of contact after the judgment with convex volume, should be judged with triangle method. Melero et al. proposed fast collision detection algorithm utilizing Extended Bounding-Planes Octree (EBP-Octree), and obtained good result [17]. In EBP-Octree, one volume node has eight children to express subspace. If each subspace has possibility to contact, this algorithm computes the contacts between recursively subspaces. Octree-based method was studied for robotics in early time [18].

Methods based on bounding volume are not available to surgical situation using CT devices, because it has the form of torus object. Therefore, the paired triangle method is adopted for contact detection between Zerobot and CT gantry without reducing the obvious outer triangles. It called brute-force method, and of course, the hybrid method is attractive to reduce the calculation time. In this paper the hybrid method is not adopted for two reasons. One is that the affect for torus object is unclear. Another is that the cost to reconstruct the tree when changing posture of the robot arm has possibility be larger. The adoption of hybrid method is a future work in this paper.

The above mentioned conventional studies have superior technique, on the other hand the real experiments with complicated shape devices is not conducted. The performance confirms contact detection with experimental evidence, which is an advantage of this paper over other papers

2. Zerobot

The overview of Zerobot and structure of end-effector are shown in Fig. 2. This robot has five degrees of freedom to decide the position and the posture of the needle, and one degree of freedom to move along puncture direction. As shown in Fig. 2, q_1, q_2, and q_3 are linear motion joints. q_4, and q_5 are, on the other hand, revolving joint, to change posture of the needle. Also, q_6 is a linear motion joint to insert a needle along with predetermined axis by q_4, and q_5. Due to the property of CT image reconstruction, metal parts on CT scanning plane cause artifacts, which are large noise blocks in CT image. It is difficult to visually recognize organs of the patient and prevents continuing surgery. Therefore, actuators and sensors are mounted far from CT scanning plane. It can be realized by applying parallel mechanism to end-effector.

2.1. Kinematics

In order to calculate the needle posture and needle tip position $\boldsymbol{r}$ from the angle and displacement $\boldsymbol{q}$ of each joint of the Zerobot, the formula of forward kinematics is derived. Here, $\sin\theta$ is expressed as S_θ, and $\cos\theta$ is expressed as C_θ for Abbreviation. First, the coordinate systems $\Sigma_W, \Sigma_0, \Sigma_1, \ldots, \Sigma_6, \Sigma_E$ are arranged as shown in Fig. 4. Because above mentioned coordinate systems are based on Denavit-Hartenberg method, by using the parameters $\alpha_{i-1}, a_{i-1}, d_i, \theta_i$ shown in Table 1, the homogeneous transformation matrix ${}^{i-1}\boldsymbol{T}_i$ from Σ_{i-1} to Σ_i can be generally expressed as in equation (1).

$$(1) \qquad {}^{i-1}\boldsymbol{T}_i = \begin{bmatrix} C_{\theta_i} & -S_{\theta_i} & 0 & a_{i-1} \\ S_{\theta_i}C_{\alpha_{i-1}} & C_{\theta_i}C_{\alpha_{i-1}} & -S_{\alpha_{i-1}} & -d_iS_{\alpha_{i-1}} \\ S_{\theta_i}S_{\alpha_{i-1}} & C_{\theta_i}S_{\alpha_{i-1}} & C_{\alpha_{i-1}} & d_iC_{\alpha_{i-1}} \\ 0 & 0 & 0 & 1 \end{bmatrix}$$

With the Denavit-Hartenberg method, we can obtain ${}^0\boldsymbol{T}_1, {}^1\boldsymbol{T}_2, \ldots, {}^5\boldsymbol{T}_6$, and finally ${}^0\boldsymbol{T}_6$ is calculated as equation (2). It should be mentioned that the parameter α_3 will be set as $+90$ degree or -90 degree depending on mounting position of Zerobot against CT gantry. In both cases, C_{α_3} equals zero. So, terms containing C_{α_3} omits from all expressions.

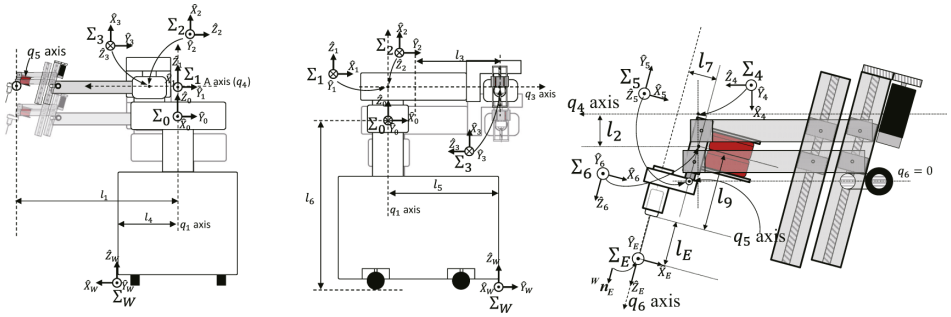

(a) Side view (b) Front view (c) End effector

Figure 4: Coordinate systems of Zerobot.

Table 1: DH parameters

i	α_{i-1}[deg]	a_{i-1}[m]	d_i[m]	θ_i [deg]
1	0	0	q_1	0
2	-90	0	q_2	-90
3	90	0	$q_3 - l_3$	0
4	90 or -90	0	l_1	$180 + q_4$
5	-90	l_2	0	$90 + q_5$
6	90	0	q_6	0

$$
\begin{aligned}
{}^0\boldsymbol{T}_6 &= {}^0\boldsymbol{T}_1 \cdot {}^1\boldsymbol{T}_2 \cdot {}^2\boldsymbol{T}_3 \cdot {}^3\boldsymbol{T}_4 \cdot {}^4\boldsymbol{T}_5 \cdot {}^5\boldsymbol{T}_6 \\
&= \begin{bmatrix} -S_{q_4}S_{q_5}S_{\alpha_3} & C_{q_4}S_{\alpha_3} & S_{q_4}C_{q_5}S_{\alpha_3} & {}^0r_{6x} \\ C_{q_5}S_{\alpha_3} & 0 & S_{q_5}S_{\alpha_3} & {}^0r_{6y} \\ C_{q_4}S_{q_5} & S_{q_4} & -C_{q_4}C_{q_5} & {}^0r_{6z} \\ 0 & 0 & 0 & 1 \end{bmatrix}
\end{aligned} \tag{2}
$$

Here,

$$
\begin{aligned}
{}^0r_{6x} &= l_3 - q_3 + l_2 S_{q_4} S_{\alpha_3} + q_6 S_{q_4} C_{q_5} S_{\alpha_3}, \\
{}^0r_{6y} &= q_6 S_{q_5} S_{\alpha_3} + q_2 - l_1 S_{\alpha_3}, \\
{}^0r_{6z} &= q_1 - l_2 C_{q_4} - q_6 C_{q_4} C_{q_5}.
\end{aligned}
$$

By adding some offsets shown in Fig. 4, the homogeneous transformation matrix ${}^W\boldsymbol{T}_E$ from world coordinate system Σ_W to needle end coordinate system Σ_E is calculated as equation (3).

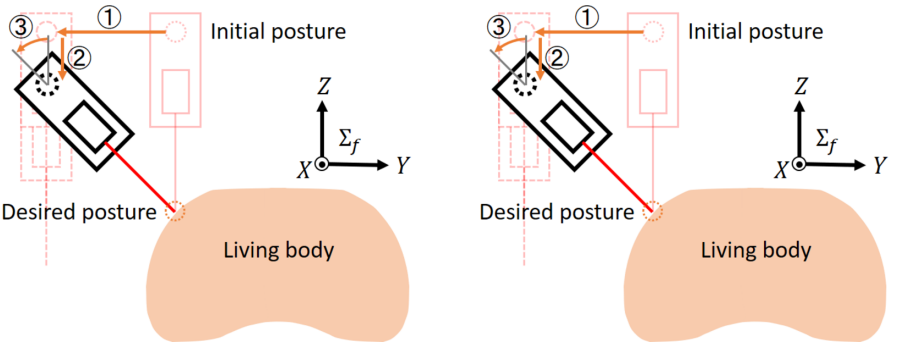

(a) Motion without remote center function (b) Motion with remote center function

Figure 5: Remote center motion.

$$
\begin{aligned}
{}^{W}\boldsymbol{T}_{E} &= {}^{W}\boldsymbol{T}_{0} \cdot {}^{0}\boldsymbol{T}_{E} \\
&= \begin{bmatrix}
-C_{q_5}S_{\alpha_3} & 0 & -S_{q_5}S_{\alpha_3} & -{}^{0}r_{Ey} - l_4 \\
-S_{q_4}S_{q_5}S_{\alpha_3} & C_{q_4}S_{\alpha_3} & S_{q_4}C_{q_5}S_{\alpha_3} & {}^{0}r_{Ex} - l_5 \\
C_{q_4}S_{q_5} & S_{q_4} & -C_{q_4}C_{q_5} & {}^{0}r_{Ez} + l_6 \\
0 & 0 & 0 & 1
\end{bmatrix}
\end{aligned} \tag{3}
$$

Here,

$$
\begin{aligned}
{}^{0}r_{Ex} &= l_3 - q_3 + l_2 S_{q_4} S_{\alpha_3} + (q_6 + l_9 + l_E)\, S_{q_4} C_{q_5} S_{\alpha_3} + l_7 S_{q_4} S_{q_5} S_{\alpha_3}, \\
{}^{0}r_{Ey} &= (q_6 + l_9 + l_E)\, S_{q_5} S_{\alpha_3} + q_2 - l_1 S_{\alpha_3} - l_7 S_{\alpha_3} C_{q_5}, \\
{}^{0}r_{Ez} &= q_1 - l_2 C_{q_4} - (q_6 + l_9 + l_E)\, C_{q_4} C_{q_5} - l_7 S_{q_5} C_{q_4}.
\end{aligned}
$$

2.2. Remote center function

In the IR procedure by the robot, the robot is operated by remote control to bring the needle tip to the puncture point above the body surface. If the robot is rotated around the needle root above the body surface as shown in Fig. 5(a), it takes a lot of time. In addition to this, there is a risk that the patient's organ or body surface may be damaged accidentally because the needle tip moves for each rotational motion command. Therefore, it is necessary to synchronize each axis and change the posture of the needle by rotating around the needle tip as shown in Fig. 5(b). This function is named as the remote center, and introduced this function in the robot [19].

3. Contact detection

3.1. Overview of detecting contact condition

To avoid those collision, we propose a contact detection algorithm between the arm part and the CT gantry. The sequence of automated IR surgery is below.

1) Zerobot is set up; that includes checking safety function.
2) The patient lays on the bed of CT equipment. Then the body is scanned with CT in order to decide the path plan of the needle insertion.
3) The path plan is decided on the console of CT system. Then the target mark for insertion needle is painted on surface of the patient based on information of the path plan.
4) The Zerobot slowly moves to initial position for the insertion.
5) Finally, the needle is inserted into target tumor of patient with checking CT fluoroscopy for safety.

In the step to decide the path plan of needle insertion, the doctor must consider contact condition between the robot arm and the environmental device. The method to detect contact condition automatically will be able to help the doctor's judgment. The sequence to detect contact condition is below.

1) The doctor sets the candidate of the path plan of needle insertion.
2) The surface triangles of the robot arm are placed in simulation space based on information of kinematics, which is calculated from the path plan.
3) The surface triangles of the CT gantry also are also placed there.
4) Finally, the contact detection algorithm is executed on all combinations of the triangles that belong to the robot part and the triangles that belong to the CT gantry, respectively.

3.2. Contact detection algorithm

By converting the three-dimensional CAD data of each part of robot into the Standard Triangulated Language (STL) data, the parts of the robot can be expressed as a set of triangles with normal vector. As shown in Fig. 6, triangles of each part are placed on world coordinate system based on kinematics, which mentioned in subsection 2.1. It should be mentioned that

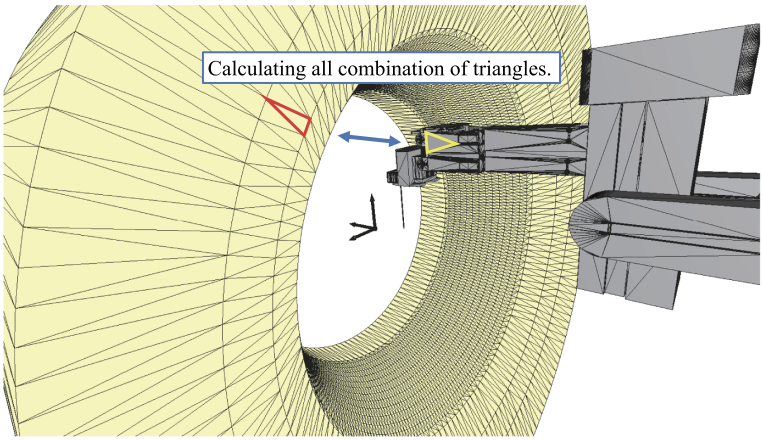

Figure 6: Triangles of both the robot and CT gantry.

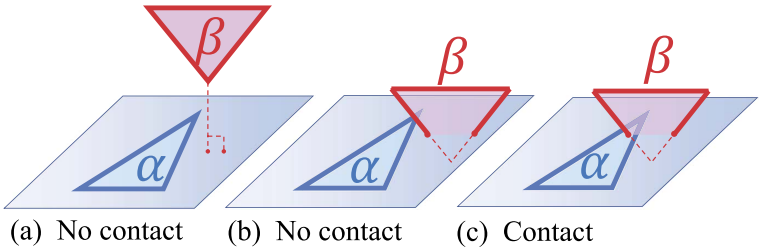

Figure 7: Three cases of contact or no contact.

some parts of end-effector do not incline against motion of angle q_5, because parallel mechanism is adopted. For those parts, homogeneous transformation matrix ${}^{W}\boldsymbol{T}_4$ is adopted for expressing posture. Also, surface of CT gantry, which is surrounding device, is converted into STL data. Contact can be judged by detecting the overlap of two triangles. It can be divided into contact state and no contact state, as shown in Fig. 7. Each point of triangles α and β is defined as shown in Fig. 8. For example, $(x_{\alpha 1}, y_{\alpha 1}, z_{\alpha 1})$ means the position of point α_1. Then, the flowchart of contact detecting algorithm is shown in Fig. 9. First, it is considered whether points $\{\beta_1, \beta_2, \beta_3\}$ exist on the same side of space that is divided by plane generated from points $\{\alpha_1, \alpha_2, \alpha_3\}$. Condition with equation (4) means that there is no contact between triangle α with triangle β as shown in Fig. 7 (a), because three points of β_1, β_2 and β_3 are in the same subspace divided by plane including

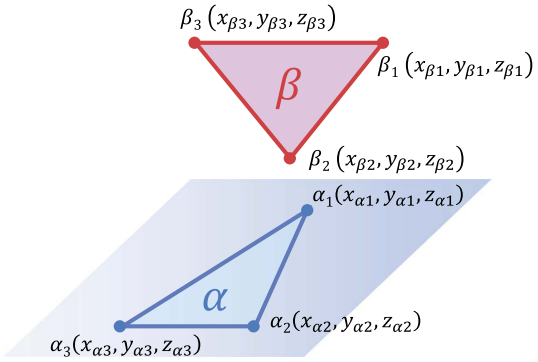

Figure 8: Definitions of triangles.

α_1, α_2 and α_3.

$$f_{(\alpha1,\alpha2,\alpha3)}(x_{\beta1}, y_{\beta1}, z_{\beta1}) f_{(\alpha1,\alpha2,\alpha3)}(x_{\beta2}, y_{\beta2}, z_{\beta2}) > 0 \quad \cap \\ f_{(\alpha1,\alpha2,\alpha3)}(x_{\beta1}, y_{\beta1}, z_{\beta1}) f_{(\alpha1,\alpha2,\alpha3)}(x_{\beta3}, y_{\beta3}, z_{\beta3}) > 0. \tag{4}$$

Here, the definition of $f_{(\alpha1,\alpha2,\alpha3)}(x, y, z)$ is written in equation (5).

$$f_{(\alpha1,\alpha2,\alpha3)}(x, y, z) = ax + by + cz + d. \tag{5}$$

Also, parameters a, b, c and d, which are coefficient to express plane including points α_1, α_2, α_3, are calculated as below.

$$\boldsymbol{r}_1 = \begin{pmatrix} x_{\alpha1} - x_{\alpha2} \\ y_{\alpha1} - y_{\alpha2} \\ z_{\alpha1} - z_{\alpha2} \end{pmatrix}, \quad \boldsymbol{r}_2 = \begin{pmatrix} x_{\alpha1} - x_{\alpha3} \\ y_{\alpha1} - y_{\alpha3} \\ z_{\alpha1} - z_{\alpha3} \end{pmatrix}, \quad \begin{pmatrix} a \\ b \\ c \end{pmatrix} = \boldsymbol{r}_1 \times \boldsymbol{r}_2,$$
$$d = -(ax_{\alpha1} + by_{\alpha1} + cz_{\alpha1}).$$

If there still remains possibility of contact of two triangles, the calculation continues as shown in Fig. 9. Secondly, it is judged whether the edge of triangle β pierces the triangle α. If one of three edges pierces another triangle, it can be thought that those triangles contact. Here, as an example with the case that the edge line $\beta_1\beta_2$ pierces the triangle α, the calculation sequence is described. With function f defined in (5), condition (6) indicates the state that edge line $\beta_1\beta_2$ goes through the triangle α. First line of the equation (6) means that α_3 and point β_2 exist in the same side of subspace that is divided by the plane including α_1, α_2 and β_1. Second and third lines of the equation (6) have same meanings for other combinations of points.

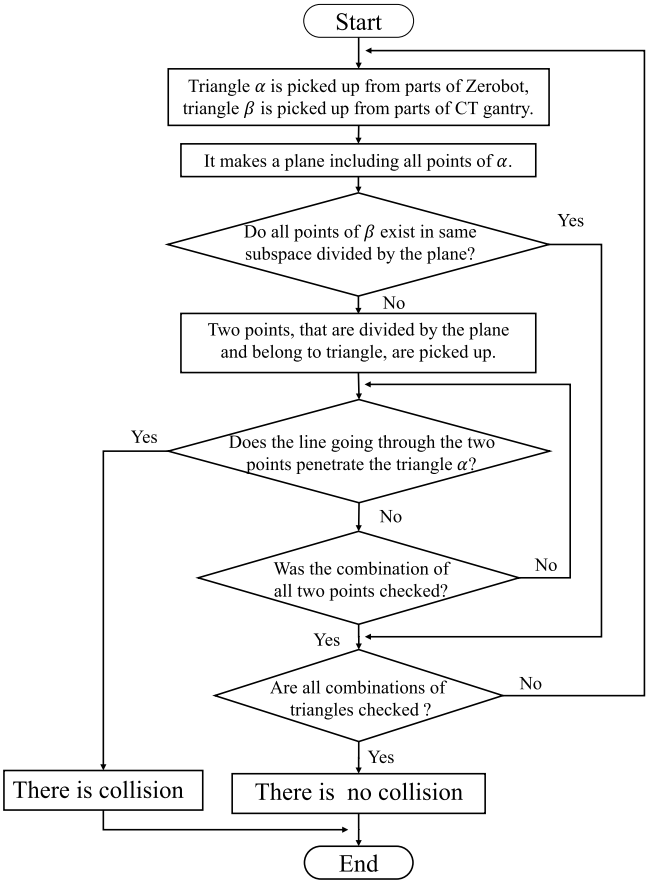

Figure 9: The flowchart of contact detection algorithm.

Examples of those situation are shown Fig. 10. When line goes through the triangle α as shown in Fig. 10(a), both a point of the line and a point of the triangle exist in same side of subspace divided by the plane including other three points for combinations of the points $\alpha_3\beta_2$, $\alpha_1\beta_2$ and $\alpha_2\beta_2$ as shown in Fig. 10(b)(c) and (d).

Even though the calculation for combination of β_1 and β_2 is described as an example, this calculation should be executed for combination of points that are divided by plane including triangle α. In the case to judge that there is collision, contact detection algorithm is finished. Otherwise, the contact detection algorithm continues until it finished checking contact of

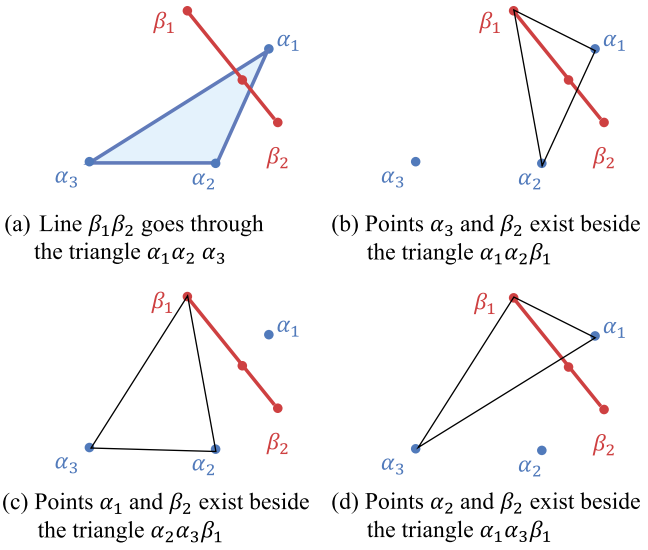

(a) Line $\beta_1\beta_2$ goes through the triangle $\alpha_1\alpha_2\ \alpha_3$

(b) Points α_3 and β_2 exist beside the triangle $\alpha_1\alpha_2\beta_1$

(c) Points α_1 and β_2 exist beside the triangle $\alpha_2\alpha_3\beta_1$

(d) Points α_2 and β_2 exist beside the triangle $\alpha_1\alpha_3\beta_1$

Figure 10: Examples of situation described with equation (6). (b) is for first line of (6), and (c) is for second line of (6), and (d) is for third line of (6).

all combination of triangles as shown flowchart in Fig. 9.

$$
\begin{aligned}
(6) \qquad & f_{(\alpha1,\alpha2,\beta1)}(x_{\beta2}, y_{\beta2}, z_{\beta2}) f_{(\alpha1,\alpha2,\beta1)}(x_{\alpha3}, y_{\alpha3}, z_{\alpha3}) > 0 \quad \cap \\
& f_{(\alpha2,\alpha3,\beta1)}(x_{\beta2}, y_{\beta2}, z_{\beta2}) f_{(\alpha2,\alpha3,\beta1)}(x_{\alpha1}, y_{\alpha1}, z_{\alpha1}) > 0 \quad \cap \\
& f_{(\alpha3,\alpha1,\beta1)}(x_{\beta2}, y_{\beta2}, z_{\beta2}) f_{(\alpha3,\alpha1,\beta1)}(x_{\alpha2}, y_{\alpha2}, z_{\alpha2}) > 0
\end{aligned}
$$

4. Experiment

In order to confirm the function of contact detection algorithm, an experiment using both of actual CT equipment and Zerobot is conducted.

4.1. Experimental condition

The experimental setup to confirm the performance of proposed contact detection using actual CT gantry is shown in Fig. 11. The observer in front of gantry is placed to tell the operator the possibility of the unexpected real contact. The observer near the simulator must check the contact condition calculated by the proposed algorithm. The operator holds the control interface to operate Zerobot, and moves Zerobot to a predetermined distance

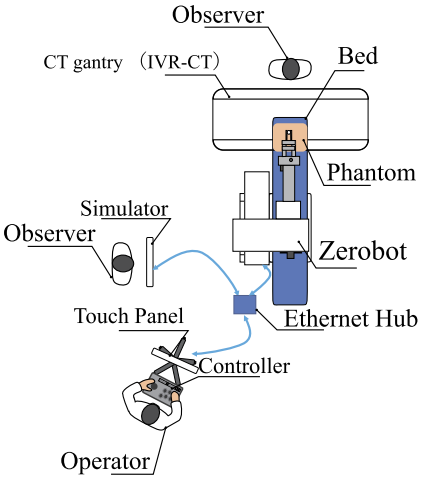

Figure 11: Experimental setup.

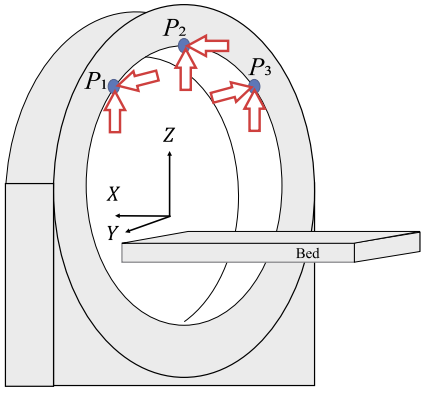

Figure 12: Goal points for contact: P_1, P_2, P_3.

for CT gantry while repeating both the measurement and the movement. The goal points for contact are indicated in Fig. 12. For the points of P_1 and P_3, the end-effector of Zerobot approaches along with Y axis and Z axis respectively in each experiment. Meanwhile, the end-effector of Zerobot approaches the point of P_2 along with X axis and Z axis respectively in each experiment.

The method to measure the distance is shown in Fig. 13. The dial caliper gauge is utilized to measure the shortest distance between Zerobot and the CT gantry. Also, the volume of Zerobot in simulation is enlarged with 20mm

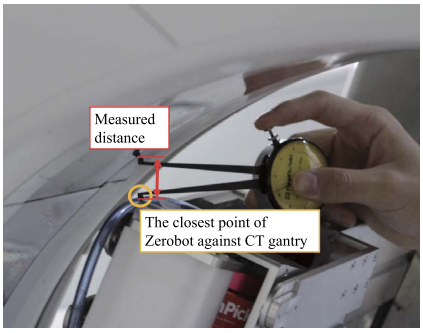

Figure 13: Appearance measuring the distance between an arm part of Zerobot and CT gantry.

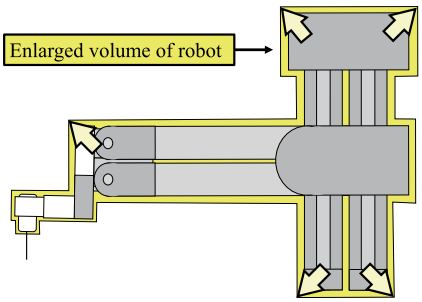

Figure 14: Enlarged volume of end-effector.

size along each axis, in order to perform the experiment with the boundary set at the position of 20 mm as below mentioned. The sequence of contact detection experiment is listed below.

1) Control system of Zerobot is booted, and Zerobot performs initialization of each joint.
2) The needle is attached in the end-effector of Zerobot.
3) A CT image of the needle tip is taken for calibration.
4) Zerobot is operated so that the needle tip position is aligned with the center of the CT gantry.
5) Zerobot is operated to move along with X or Y or Z axis, so as to make the distance between the end-effector and the closest part of the CT gantry to 25 mm.
6) The contact judgment is conducted for confirmation that contact between the end-effector and gantry do not occur yet.

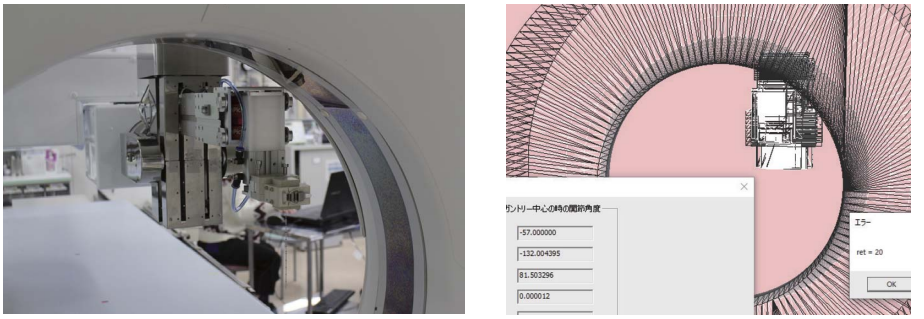

(a) Experiment with actual CT-gantry (b) Visualized simulation

Figure 15: Appearance of experiment.

7) Zerobot is operated to make the distance between the hand part and the closest part of the CT gantry to 15 mm.

Because the safety margin is set as 20mm, proposed algorithm in above contact judgment experiment with 25-mm distance should correctly generate the judgment of no contact. In contrast, that with 15-mm distance should correctly generate the judgment that contact of end-effector occurs.

4.2. Experimental result

The appearance of the experiment is shown Fig. 15. The end-effector of Zerobot approaches to CT gantry is shown in Fig. 15(a), and visualized simulation displays same situation by receiving position data from Zerobot as shown in Fig. 15(b). Experimental results for point P_1 for various posture of end-effector are shown in table 2. The "✓" mark means in condition of measured distance d_m equaling 25mm that the algorithm correctly made judgment of no contact between Zerobot and CT gantry. If not, "×" is marked in the table. Meanwhile, the "✓" mark means in condition of distance d_m equaling 15mm that the algorithm estimated that there is contact between Zerobot and CT gantry. If not, "×" is marked in the table. Totally, contact detection worked correctly in 22 times against 24 trials for point P_1.

Experimental results for point P_2 for various posture of end-effector are shown in Table 3. The case of approaching along X axis, which is shown in Fig. 16, has only four experiments. Because the condition that upper cover contacts point P_2 is limited. The meanings of "✓" and "×" are same in the Table 2. Totally, proposed contact detection algorithm worked correctly in 15 times against 16 trials for point P_2.

Table 2: The results of contact detection for point P_1: The "✓" mark means that contact detection algorithm worked correctly. Meanwhile, the "×" mark means the algorithm misrecognized the contact condition

Experimental condition		Moving along Y axis		Moving along Z axis	
Posture of end-effector		Result for distance		Result for distance	
q_4 [deg]	q_5 [deg]	$d_m = 25$mm	$d_m = 15$mm	$d_m = 25$mm	$d_m = 15$mm
0 deg	0 deg.	✓	✓	✓	✓
30 deg	0 deg.	✓	✓	✓	✓
−30 deg	0 deg.	✓	✓	✓	✓
0 deg	15 deg.	✓	✓	✓	✓
30 deg	15 deg.	✓	✓	✓	✓
−30 deg	−15 deg.	✓	×	✓	×

Table 3: The results of contact detection for point P_2: "–" means that there is no measurement with the condition

Experimental condition		Moving along X axis		Moving along Z axis	
Posture of end-effector		Result for distance		Result for distance	
q_4 [deg]	q_5 [deg]	$d_m = 25$mm	$d_m = 15$mm	$d_m = 25$mm	$d_m = 15$mm
0 deg	0 deg.	-	-	✓	✓
30 deg	0 deg.	-	-	✓	✓
−30 deg	0 deg.	-	-	✓	✓
0 deg	15 deg.	✓	✓	✓	✓
30 deg	15 deg.	✓	✓	✓	✓
−30 deg	−15 deg.	-	-	✓	×

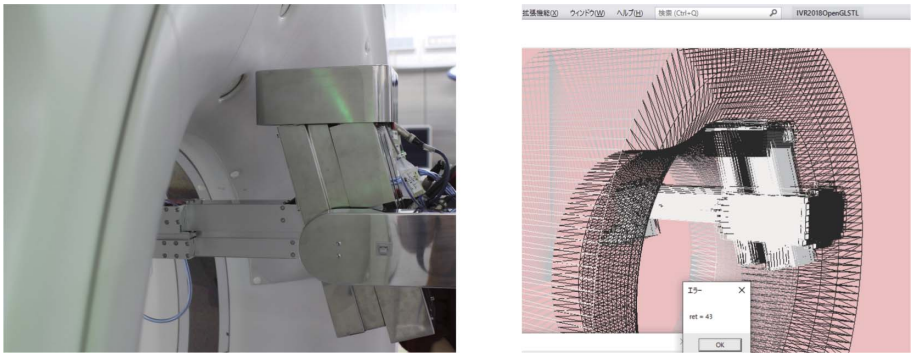

(a) Experiment with actual CT-gantry (b) Visualized simulation

Figure 16: Appearance of experiment approaching along X axis for point P_2.

Table 4: The results of contact detection for point P_3

Experimental condition		Moving along Y axis		Moving along Z axis	
Posture of end-effector		Result for distance		Result for distance	
q_4 [deg]	q_5 [deg]	$d_m = 25$mm	$d_m = 15$mm	$d_m = 25$mm	$d_m = 15$mm
0 deg	0 deg.	✓	✓	✓	✓
30 deg	0 deg.	✓	✓	✓	✓
−30 deg	0 deg.	✓	✓	✓	✓
0 deg	15 deg.	✓	✓	✓	×
30 deg	15 deg.	✓	×	✓	×
−30 deg	−15 deg.	✓	✓	✓	×

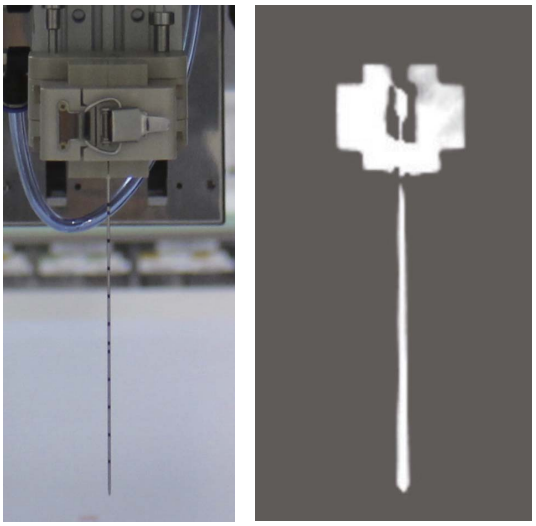

(a) Actual (b) CT image

Figure 17: Image of needle held by Zerobot.

Finally, experimental results for point P_3 for various posture of end-effector are shown in Table 4. Totally, proposed contact detection algorithm worked correctly in 20 times against 24 trials for point P_3.

4.3. Discussion

We have found two reasons why proposed algorithm fails to estimate correct contact condition. One is the calibration method, which was conducted in the sequence of experiment. We used the CT image of the needle held by Zerobot as shown in Fig. 17. Originally, the diameter of the needle is approximately 1.1 mm. Meanwhile, the width of the needle in CT image was

approximately 5mm by effect of metal artifact. So, there is the possibility to generate some deviation when pointing the needle edge point on the screen. Other is deflection of end-effector, because the length of end-effector of Zerobot is approximately 900mm. Their length is required for matching current CT gantry that has large depth to CT scanning plane from the front side of gantry. Meanwhile, it will generate deformation of beams of end-effector depending on posture of Zerobot.

5. Conclusion

In this paper, in order to avoid the collision between Zerobot and CT gantry during the automated puncturing, the algorithm to detect the contact between Zerobot and CT gantry was proposed. First, we obtained 3D STL data for each part of the robot hand from the robot drawing using 3D CAD software. Secondly, each component was placed in space on the simulation based on the kinematics of the parallel link mechanism using the homogeneous transformation matrix. Then, we proposed a contact detection algorithm for triangles on a three-dimensional space, which is the minimum element of STL data. So as to confirm the performance of contact detection algorithm, experiments using actual CT gantry and Zerobot were conducted. The success rate of the contact detection experiments reached 89% for 64 trials with various posture of end-effector. We plan to improve the performance of contact detection by revising the calibration method for enough durability in actual usage.

References

[1] T. Fukuda, S. Guo, K. Kosuge, F. Arai, M. Negoro and K. Nakabayashi, "Micro active catheter system with multi degrees of freedom," Proceedings of the 1994 IEEE International Conference on Robotics and Automation, 1994, pp. 2290–2295, vol. 3, doi: 10.1109/ROBOT.1994.350944.

[2] S. Guo, T. Fukuda, T. Nakamura, F. Arai, K. Oguro and M. Negoro, "Micro active guide wire catheter system-Characteristic evaluation, electrical model and operability evaluation of micro active catheter," Proceedings of IEEE International Conference on Robotics and Automation, 1996, pp. 2226–2231, vol. 3, doi: 10.1109/ROBOT.1996.506495.

[3] M. Tanimoto, F. Arai, T. Fukuda and M. Negoro, "Augmentation of safety in teleoperation system for intravascular neurosurgery: a new control strategy for force display based on the variable impedance characterization," Proceedings of IEEE International Conference on Robotics and Automation, Leuven, Belgium, 1998, pp. 2890–2895, vol. 4.

[4] M. Tanimoto, F. Arai, T. Fukuda and M. Negoro, "Force display method to improve safety in teleoperation system for intravascular neurosurgery," Proceedings of IEEE International Conference on Robotics and Automation, Detroit, MI, USA, 1999, pp. 1728–1733, vol. 3.

[5] S. Ikeda, F. Arai, T. Fukuda et al., "In vitro patient-tailored anatomical model of cerebral artery for evaluating medical robots and systems for intravascular neurosurgery," 2005 IEEE/RSJ International Conference on Intelligent Robots and Systems, 2005, pp. 1558–1563, doi: 10.1109/IROS.2005.1545554.

[6] S. Ikeda, C. Tercero, T. Fukuda, Y. Okada, F. Arai, M. Negoro, M. Hayakawa, I. Takahashi "Patient-Specific IVR Endovascular Simulator with Augmented Reality for Medical Training and Robot Evaluation," Journal of Robotics and Mechatronics, Fuji Technology Press, 2008, 20(3):441–448.

[7] Takao Hiraki, Tetsushi Kamegawa, Takayuki Matsuno, Susumu Kanazawa, "Development of a Robot for CT Fluoroscopy-guided Intervention: Free Physicians from Radiation", J Intervent Radiol, 2014, 20:375–381.

[8] D. Staianovici, K. Cleary, A. Patriciu, D. Mazilu, A. Stanimir, N. Craciunoiu, V. Watson, L. Kavoussi, "AcuBot: A Robot for Radiological Interventions," IEEE Transaction on Robotics and Automation, 2003, 19(5):927–930.

[9] B. Maurin, B. Bayle, O. Piccin, J. Ganglo, M. Mathelin, C. Doignon, P. Zanne, A. Gangi, "A Patient-Mounted Robotic Platform for CT-Scan Guided Procedures," IEEE Transaction on Biomedical Engineering, 2008, 55(10):2417–2425.

[10] Y. Koethe, S. Xu, G. Velusamy, B. J. Wood, A. M. Venkatesan, "Accuracy and efficacy of percutaneous biopsy and ablation using robotic assistance under computed tomography guidance: a phantom study," European Radiology, 2013, 24(3):723–730.

[11] Takao Hiraki, et al. "Robotically Driven CT-guided Needle Insertion: Preliminary Results in Phantom and Animal Experiments," Radiology, 2017, 162856.

[12] Christer Ericson, "Real-Time Collision Detection," CRC Press, 2004, ISBN: 1558607323.

[13] Bolun Wang, Zachary Ferguson, Teseo Schneider, Xin Jiang, Marco Attene, Daniele Panozzo, "A Large-scale Benchmark and an Inclusion-based Algorithm for Continuous Collision Detection," ACM Transactions on Graphics, 2021, 40(5):188:1–188:16.

[14] A. P. del Pobil, M. A. Serna and J. Llovet, "A new representation for collision avoidance and detection," Proceedings 1992 IEEE International Conference on Robotics and Automation, 1992, 1:246–251.

[15] Tomas Moller, "A Fast Triangle-Triangle Intersection Test," Journal of Graphics Tools, 1997, 2(2):25–30, DOI: 10.1080/10867651.1997.10487472.

[16] René Weller, Nicole Debowski, Gabriel Zachmann, "kDet: Parallel Constant Time Collision Detection for Polygonal Objects," Computer Graphics Forum, 2017, 36(2):131–141.

[17] Francisco J. Melero, Angel Aguilera, Francisco Ramon Feito, "Fast collision detection between high resolution polygonal models," Computer & Graphics, 2019, 83:97–106.

[18] D. Jung and K. K. Gupta, "Octree-based hierarchical distance maps for collision detection," Proceedings of IEEE International Conference on Robotics and Automation, 1996, 1:454–459.

[19] Kohei Sugiyama, Takayuki Matsuno, Tetsushi Kamegawa, Takao Hiraki, Hirotaka Nakaya, Masayuki Nakamura, Akira Yanou, and Mamoru Minami, "Needle Tip Position Accuracy Evaluation Experiment for Puncture Robot in Remote Center Control," Journal of Robotics and Mechatronics, 2016, 28(6).

T. Matsuno
Graduate School of Natural Science and Technology
Okayama University
Tsushimanaka 3-1-1 Kita-ku
Okayama City, Okayama
Japan
E-mail address: matsuno@okayama-u.ac.jp

N. Kido
Graduate School of Natural Science and Technology
Okayama University
Tsushimanaka 3-1-1 Kita-ku
Okayama City, Okayama
Japan
E-mail address: p2la8jiy@s.okayama-u.ac.jp

T. Kamegawa
Graduate School of Interdisciplinary Science
and Engineering in Health Systems
Okayama University
Tsushimanaka 3-1-1 Kita-ku
Okayama City, Okayama
Japan
E-mail address: kamegawa@okayama-u.ac.jp

T. Hiraki
Graduate School of Medicine
Dentistry and Pharmaceutical Sciences
Okayama University
Shikata-cho 2-5-1 Kita-ku
Okayama City, Okayama, Japan
E-mail address: hiraki-t@cc.okayama-u.ac.jp

T. Fukuda
Graduate School of Science and Technology
Meijo University
1-501 Shiogamaguchi, Tempaku-ku
Nagoya, Aichi
Japan
E-mail address: tofukuda@meijo-u.ac.jp

Received September 8, 2020